Flagellar Perturbations Activate Adhesion through Two Distinct Pathways in *Caulobacter crescentus*

David M. Hershey,[b] [ID] Aretha Fiebig,[a] [ID] Sean Crosson[a]

[a]Department of Microbiology and Molecular Genetics, Michigan State University, East Lansing, Michigan, USA
[b]Department of Biochemistry and Molecular Biology, University of Chicago, Chicago, Illinois, USA

ABSTRACT   Bacteria carry out sophisticated developmental programs to colonize exogenous surfaces. The rotary flagellum, a dynamic machine that drives motility, is a key regulator of surface colonization. The specific signals recognized by flagella and the pathways by which those signals are transduced to coordinate adhesion remain subjects of debate. Mutations that disrupt flagellar assembly in the dimorphic bacterium *Caulobacter crescentus* stimulate the production of a polysaccharide adhesin called the holdfast. Using a genomewide phenotyping approach, we compared surface adhesion profiles in wild-type and flagellar mutant backgrounds of *C. crescentus*. We identified a diverse set of flagellar mutations that enhance adhesion by inducing a hyperholdfast phenotype and discovered a second set of mutations that suppress this phenotype. Epistasis analysis of the *flagellar signaling suppressor* (*fss*) mutations demonstrated that the flagellum stimulates holdfast production via two genetically distinct pathways. The developmental regulator PleD contributes to holdfast induction in mutants disrupted at both early and late stages of flagellar assembly. Mutants disrupted at late stages of flagellar assembly, which assemble an intact rotor complex, induce holdfast production through an additional process that requires the MotAB stator and its associated diguanylate cyclase, DgcB. We have assigned a subset of the *fss* genes to either the stator- or *pleD*-dependent networks and characterized two previously unidentified motility genes that regulate holdfast production via the stator complex. We propose a model through which the flagellum integrates mechanical stimuli into the *C. crescentus* developmental program to coordinate adhesion.

IMPORTANCE Understanding how bacteria colonize solid surfaces is of significant clinical, industrial and ecological importance. In this study, we identified genes that are required for *Caulobacter crescentus* to activate surface attachment in response to signals from a macromolecular machine called the flagellum. Genes involved in transmitting information from the flagellum can be grouped into separate pathways, those that control the *C. crescentus* morphogenic program and those that are required for flagellar motility. Our results support a model in which a developmental and a mechanical signaling pathway operate in parallel downstream of the flagellum and converge to regulate adhesion. We conclude that the flagellum serves as a signaling hub by integrating internal and external cues to coordinate surface colonization and emphasize the role of signal integration in linking complex sets of environmental stimuli to individual behaviors.

KEYWORDS adhesion, flagellum, motility, holdfast, biofilm

For microorganisms, solid surfaces serve as sites of nutrient accumulation, gateways into host tissues and shelters from environmental stresses (1–3). To access surface-associated niches, bacteria deploy specialized programs for seeking, recognizing, and colonizing objects in their surroundings (4). These programs culminate in a pronounced transition away from a free-living, exploratory state and toward an adherent,

FIG 1 Identifying genes that link the flagellum to holdfast production. (A) Asymmetric division cycle of *C. crescentus*. Sessile stalked cells divide to release a newborn swarmer cell that displays a flagellum and type IV pili. Quiescent swarmer cells undergo a morphological transition to become replication competent stalked cells. Transitioning swarmer cells can make an adhesin called the holdfast (red) that promotes surface attachment. (B) Schematic of flagellar architecture. A central hook-basal body (HBB) complex (blue) spanning the cell envelope tethers a long extracellular filament (purple) to the surface of the cell. Multiple stator subunits (gold) that surround the inner membrane embedded rotor (teal) use ion translocation to turn the HBB and its associated filament. Outer membrane (OM), peptidoglycan (PG), and inner membrane (IM) layers of the envelope are shown. (C) The Δ*flgH* mutant shows increased surface colonization (top), as measured by crystal violet (CV) staining, and a higher proportion of holdfast-producing cells relative to the wild type (bottom). Holdfasts were stained with Alexa-594–wheat germ agglutinin (fWGA). (D) Hyper-adhesive mutants identified by adhesion profiling in defined medium. The 75 genes with the strongest hyperadhesive profiles are plotted, and specific flagellar assembly genes are highlighted. The colors correspond to the structural proteins depicted in panel B. The plotted genes are listed in Table S1. (E) The flagellar signaling suppressor (*fss*) genes identified by adhesion profiling in the Δ*flgH* background. The 50 genes with the strongest contributions to adhesion in the Δ*flgH* background are plotted. *hfsA*, a gene required for holdfast biosynthesis, is highlighted, along with two *fss* genes, *pleD* and *motB*. The plotted genes are listed in Table S2. For panels D and E, each line represents the average fitness values for a single gene plotted as a function of time in the sequential passaging experiment. Hyperadhesive mutants are depleted more rapidly than neutral mutants during selection in cheesecloth. Mutated genes (*fli*, *flg*, *flm*, etc.) that display increased attachment to cheesecloth show steadily decreasing fitness scores as a function of passage number. Mutants with reduced adhesion are enriched in broth when grown with cheesecloth. Mutated genes that display decreased adhesion (*hfs* and *fss*) show steadily increasing fitness scores.

sessile lifestyle (5–7). Sophisticated signaling networks that integrate a host of environmental cues are used to coordinate the motile-to-sessile switch (8–10). The complexity of these circuits reflects the perilous nature of committing to colonization programs under suboptimal conditions.

A transenvelope machine called the flagellum drives cellular motility and plays a critical role at numerous stages of surface colonization (11, 12). The flagellum is synthesized in a stepwise process that is controlled by a transcriptional hierarchy (13). Assembly begins with the expression of class II genes that code for a rotor and secretion subcomplex that are inserted in the cytoplasmic membrane (14, 15). Upon completion of the class II program, assembly proceeds outward with the incorporation of an envelope spanning basal body (class III genes), followed by the secretion of an extracellular filament (class IV genes) (16, 17). Stator subcomplexes that surround the rotor utilize ion gradients across the cytoplasmic membrane to generate torque by turning the hook-basal body complex and its associated filament, propelling the cell forward (Fig. 1) (18, 19). Flagellar motors are highly attuned to environmental conditions. They support motility under diverse conditions, modulate torque in response to changing loads and alter rotational bias to support complex swimming patterns (20–23).

Paradoxically, flagellar motility must be repressed during sessile growth but is also required for efficient surface colonization (6, 24–26). During the initial stages of

attachment, swimming is thought to promote productive interactions with target substrates by providing energy needed to overcome repulsive forces at the liquid-solid interface (27). The flagellum also plays an additional regulatory role in activating the motile-to-sessile transition by recognizing physical contact with solid substrates (11). Such tactile sensing events serve as critical cues for initiating colonization programs, but the mechanistic basis for how bacteria sense and respond to physical stimuli remains controversial.

The dimorphic bacterium *Caulobacter crescentus* is uniquely adapted to surface colonization. Cell division in *C. crescentus* is asymmetric and yields to two distinct cell types (28). Newborn swarmer cells are flagellated, produce type IV pili (T4P) and cannot initiate replication (29, 30). These motile cells undergo a morphogenic transition to become replication-competent stalked cells by replacing their flagellum and pili with a specialized envelope extension called the stalk (31). During the swarmer-to-stalked transition, *C. crescentus* can produce a polysaccharide adhesin called the holdfast that is displayed at the tip of the stalked cell, where it promotes attachment to surfaces (Fig. 1) (7, 32). Holdfast production is the primary determinant of surface colonization in *C. crescentus*, and its regulation is elaborate (26, 33). In addition to cell cycle cues (7, 34), nutrient availability (35), light (36), and redox status (37), mechanical contact has been implicated as an important activator of holdfast assembly (38). Recent evidence suggests that both flagella and T4P can stimulate holdfast production in response to contact with a surface (39, 40), but conflicting models have emerged for how these transenvelope machines survey and disseminate mechanical information (34, 41).

Here, we used an unbiased phenotyping approach called adhesion profiling to show that a diverse set of flagellar mutations induce a hyperholdfast phenotype and to identify dozens of *flagellar signaling suppressor* (*fss*) genes that contribute to holdfast stimulation downstream of the flagellum. *fss* mutations suppress the hyperadhesive effects of flagellar disruption through two distinct pathways. Select regulators of cell cycle progression are involved in stimulating adhesion upon flagellar disruption, while components of the stator subcomplexes contribute to holdfast stimulation specifically in mutants that can assemble an inner membrane rotor. We assigned roles for two previously uncharacterized genes roles in the stator-dependent pathway and demonstrated that they promote the ability of the stator subunits to turn the flagellar filament. Our results provide new insight into load sensing by the *C. crescentus* motor and highlight a novel link between flagellar assembly and morphogenesis. We propose a broad role for the flagellum in coordinating cellular physiology through its role as a signaling hub that integrates internal and external cues.

RESULTS

A complex gene network links the flagellum to holdfast production. We previously described a method called adhesion profiling by which a barcoded transposon library is sequentially passaged in the presence of a cellulose-based substrate. Adhesive mutants become depleted as they colonize the substrate, enriching for mutants with attachment defects in the surrounding broth. By monitoring the mutant population over time, we quantified each gene's contribution to adhesion at the genome scale (33). This initial study identified a set of hyperadhesive mutants that included genes involved in flagellar assembly, which suggested the presence of a specific signaling pathway linking cues from the flagellum to holdfast production (Fig. 1C). We modified our genetic selection to identify a broader range of adhesion-activating mutations by using a defined medium (M2X) in which holdfast production is almost entirely repressed in wild-type *C. crescentus* (35). Under these conditions, dozens of genes displayed adhesion profiles indicative of hyper-adhesion (Fig. 1D; see also Table S1 in the supplemental material). Though numerous functional categories were represented in this gene set, the overwhelming majority of hyperadhesive phenotypes were observed in mutants with predicted disruptions to flagellar assembly, chemotaxis or other flagellar processes.

We focused on the holdfast phenotype for a mutant ($\Delta flgH$) lacking the gene for the flagellar L-ring protein (42) growing in M2X medium (Fig. 1C). Consistent with previous reports (33, 34), crystal violet (CV) staining of surface attached cells was elevated in $\Delta flgH$ cultures relative to the wild type, and a larger proportion of cells displayed a holdfast when stained with fluorescently labeled wheat germ agglutinin (fWGA; Fig. 1C). Mutating genes that code for extracellular components of the *C. crescentus* flagellum was proposed to increase adhesion by rendering cells hypersensitive to surface contact (40), but our results indicated that the $\Delta flgH$ mutant displayed elevated holdfast production when grown in liquid without an activating surface. Although our standard fWGA staining protocol includes brief centrifugation steps, we confirmed that the proportion of holdfast-producing cells did not change when centrifugation was omitted and cells were imaged directly from liquid cultures (see Fig. S1). In addition, we found that the $\Delta flgH$ mutant released holdfast polysaccharide directly into spent liquid medium (see Fig. S1), another hallmark of surface-independent holdfast activation (43). These results are inconsistent with the model that the $\Delta flgH$ mutant is hypersensitive to surface contact. Instead, elevated adhesion in the $\Delta flgH$ mutant results from surface contact-independent increases in both the proportion of cells that assemble a holdfast and the amount of secreted holdfast polysaccharide. We conclude that flagellar mutations act as gain of function activators of holdfast production.

To dissect potential pathways linking the flagellum to holdfast production, we constructed a barcoded Tn-*Himar1* library in a $\Delta flgH$ background and performed a second adhesion profiling experiment with the goal of identifying mutations that suppress the hyperholdfast phenotype. As in the wild type, genes required for holdfast synthesis (*hfs*) were the strongest determinants of adhesion in the $\Delta flgH$ mutant. In addition, we identified a few dozen genes (called *fss* for flagellar signaling suppressor) that contribute to adhesion specifically in the $\Delta flgH$ background (Fig. 1E; see also Table S2). While, many of the *fss* genes are uncharacterized, insertions in genes known to promote flagellar rotation, chemotaxis, cell cycle progression, and other physiological processes had *fss* phenotypes as well. Both the abundance and the functional diversity of the suppressors point to a complex signaling network that links adhesion to flagellar motility.

Distinct adhesion patterns in flagellar assembly mutants. Two of the *fss* genes, *motB* and *pleD*, are known to regulate holdfast production under specific conditions. *motB*, which codes for one of the flagellar stator proteins, is required for rapid holdfast synthesis after surface contact in microfluidic chambers (40). *pleD*, which codes for a diguanylate cyclase that regulates morphogenesis during the swarmer-to-stalked transition (44), contributes to increased holdfast production in a flagellar hook mutant background through a process independent of surface contact (34). Previous examinations of these two genes have produced conflicting models for how surface contact, flagellar assembly, and filament rotation modulate holdfast production. Identifying mutations in both *pleD* and *motB* as suppressors of $\Delta flgH$ suggested that we could clarify the signaling pathway that links flagellar perturbations to holdfast production.

We used CV staining to examine how disrupting *pleD* and *motB* affects adhesion to polystyrene in various flagellar mutant backgrounds. Disrupting the early stages of flagellar assembly by deleting the class II genes *fliF* and *fliM* led to a hyperadhesive phenotype that was strongly suppressed by deletion of *pleD* but that was not affected by deletion of *motB*. In contrast, when holdfast production was stimulated by deletion of the class III gene *flgH* or disruption of flagellin secretion ($\Delta flmA$) (45), the hyperadhesive phenotype was suppressed by introducing either a *pleD* or a *motB* deletion (Fig. 2A). Thus, flagellar mutants stimulate adhesion through different mechanisms. Mutants that disrupt the early stages of assembly activate holdfast production through *pleD*, while mutants in which assembly is stalled at later stages stimulate adhesion through both *pleD* and *motB*.

Two pathways modulate holdfast production downstream of the flagellum. The distinct suppression patterns in *pleD* and *motB* mutants indicated that multiple pathways function downstream of the flagellum to influence adhesion. Indeed,
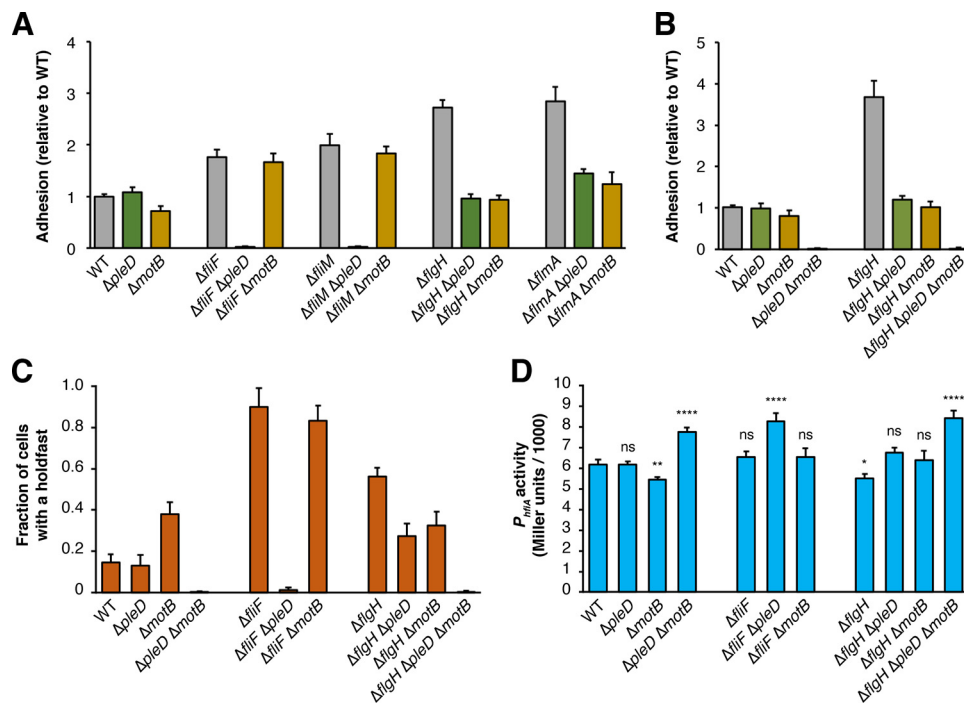
FIG 2 Two distinct signaling pathways operate downstream of the flagellum to control adhesion. (A) Crystal violet (CV)-based attachment assay showing suppression of the hyperadhesive phenotypes by *pleD* and *motB* in early (Δ*fliF* and Δ*fliM*) and late (Δ*flgH* and Δ*flmA*) flagellar assembly mutants. Mean values from six biological replicates are shown with error bars representing the associated standard deviations. (B) CV-based attachment assay showing the additive effects of Δ*motB* and Δ*pleD* on adhesion in the wild-type (WT) and Δ*flgH* backgrounds. Mean values from five biological replicates are shown with the associated standard deviations. (C) Fractions of cells with a holdfast in flagellar mutant and suppressor backgrounds. Holdfasts were stained and counted from log phase cultures as described in Materials and Methods. (D) *hfiA* transcription in flagellar mutant and suppressor backgrounds as measured by β-galactosidase activity from a P_{hfiA}-*lacZ* reporter. Mean values from three biological replicates collected on two separate dates for a total of six replicates are shown with the associated standard deviations. Statistical significance was evaluated with ANOVA followed by Tukey's multiple-comparison test. Significance compared to wild-type is indicated above each bar. ns, not significant; *, $P < 0.1$; **, $P < 0.01$; ****, $P < 0.0001$. A full statistical analysis of the CV staining, holdfast count, and LacZ activity measurements is reported in Table S3.

combining the Δ*pleD* and Δ*motB* mutations reduced CV staining to near undetectable levels in both the wild-type and Δ*flgH* backgrounds, supporting the model that *pleD* and *motB* control attachment through distinct mechanisms (Fig. 2B; see also Fig. S2A). The severe adhesion defect observed for the Δ*pleD* Δ*motB* double mutant demonstrates that the *pleD*- and *motB*-dependent pathways do not operate exclusively in the context of flagellar mutants. Either the *pleD* or the *motB* pathway must be intact for *C. crescentus* to colonize surfaces.

We quantified holdfast production by staining cells from a representative panel of mutants with fWGA. The proportion of cells displaying a holdfast was elevated in both early (Δ*fliF*) and late (Δ*flgH*) flagellar assembly mutants, and the suppression patterns seen by CV staining were recapitulated with fWGA staining. Holdfast production was elevated to similar levels in Δ*fliF* and Δ*fliF* Δ*motB* mutants but nearly eliminated in the Δ*fliF* Δ*pleD* mutant. Introducing either the Δ*pleD* or the Δ*motB* mutation reduced holdfast production in a Δ*flgH* background, and holdfast production was nearly undetectable in Δ*pleD* Δ*motB* and Δ*flgH* Δ*pleD* Δ*motB* cultures (Fig. 2C; see also Table S3). We did identify modest discrepancies between the holdfast production and polystyrene colonization measurements. Although surface attachment was indistinguishable from the wild type in Δ*motB* cultures, holdfast production in this mutant was elevated. This finding agrees with previous measurements indicating that nonmotile strains display holdfast-independent surface colonization defects (33, 34). Separately, CV staining was

higher in Δ*flgH* cultures than in Δ*fliF* cultures, but the proportion of holdfast-producing cells was higher in the Δ*fliF* mutant. Because both strains are nonmotile, the discrepancy is likely due to modulation of additional holdfast-independent colonization factors such as type IV pilus dynamics (33, 46).

Finally, we examined expression of the *holdfast inhibitor A* (*hfiA*) gene, a key regulator that inhibits adhesion by targeting a glycosyltransferase in the holdfast biosynthesis pathway (Fig. 2D) (35). Increased holdfast production in the Δ*flgH* and Δ*motB* backgrounds is accompanied by a decrease in P_{hifA}-*lacZ* reporter activity, but elevated holdfast production in the Δ*fliF* mutant occurs without a reduction in *hfiA* transcription (Fig. 2D; see also Table S3). Introducing either the Δ*motB* or Δ*pleD* mutations into the Δ*flgH* background restored P_{hifA} activity to wild-type levels. These measurements show that *pleD* is required for downregulation of *hfiA* in the Δ*flgH* background but do not clarify the role of *motB*. It remains unclear how the Δ*motB* mutation attenuates *hfiA* promoter activity in the wild-type background but restores normal expression in a Δ*flgH* mutant. Transcription from the *hfiA* promoter was elevated in Δ*pleD* Δ*motB*, Δ*flgH* Δ*pleD* Δ*motB*, and Δ*fliF* Δ*pleD* mutants, indicating that activation of *hfiA* expression contributes to the severe holdfast production defect in these three strains.

Transcription of *hfiA* is finely tuned by a complex hierarchy of transcription factors such that small changes in expression have significant impacts on holdfast production (33, 35, 37). The three nonadhesive mutants analyzed in Fig. 2 display robust increases in *hfiA* expression, and the Δ*fliF* mutant shows a striking increase in holdfast production that clearly occurs independently of *hfiA* regulation. However, P_{hifA}-*lacZ* activity differences for other key strains are modest and do not correlate perfectly with direct measurements of holdfast production. While cell cycle control and posttranscriptional processes can be masked in bulk reporter measurements, the expression level changes in flagellar signaling mutants are less pronounced than for regulatory systems that target *hfiA* directly (35, 37). A significant portion of adhesion control exerted by the flagellum likely occurs independently of *hfiA* regulation.

Parsing regulatory networks with epistasis analysis. The distinct activation profiles observed in early and late flagellar assembly mutants were used to assign *fss* genes to either the *pleD*- or *motB*-dependent signaling pathways. We predicted that *pleD* and other genes involved in stalked cell morphogenesis make up a "developmental" signaling pathway and that genes associated with stator activity make up a second, "mechanical" pathway. This model predicts that developmental pathway mutants should block holdfast stimulation in both early and late flagellar assembly mutant backgrounds, while mechanical pathway mutants should suppress hyperadhesion specifically in late assembly mutants. Two additional *fss* genes, *shkA* and *dgcB*, were used to test these predictions. *shkA* encodes a histidine kinase that regulates stalk development (47), and *dgcB* codes for a diguanylate cyclase that physically associates with stator subcomplexes (40). Deleting *shkA* suppressed the hyperadhesive effects of both Δ*fliF* (early) and Δ*flgH* (late) mutations, while deleting *dgcB* suppressed adhesion in the Δ*flgH* background but had no effect in the Δ*fliF* background (Fig. 3A). Furthermore, adhesion was nearly eliminated when the Δ*shkA* mutation was introduced into the Δ*motB* or Δ*dgcB* backgrounds (see Fig. S2), confirming that *shkA* signals through a mechanism distinct from that of mechanical pathway genes. These results provide further support for a model in which both a developmental pathway associated with stalked cell morphogenesis and a mechanical pathway associated with stator activity function downstream of the flagellum to activate adhesion.

We also used epistasis to place two uncharacterized genes identified as Δ*flgH* suppressors into the mechanical signaling pathway. *fssA* (*CC_1064*; *CCNA_01117*) encodes a protein with a Sec/SP1 secretion signal and no predicted functional domains. *fssB* (*CC_2058*; *CCNA_02137*) encodes a protein with a Sec/SP1 secretion signal and a predicted tetratricopeptide repeat (TPR) domain. Deleting either *fssA* or *fssB* did not affect adhesion in the wild-type or Δ*fliF* backgrounds but suppressed the hyperadhesive
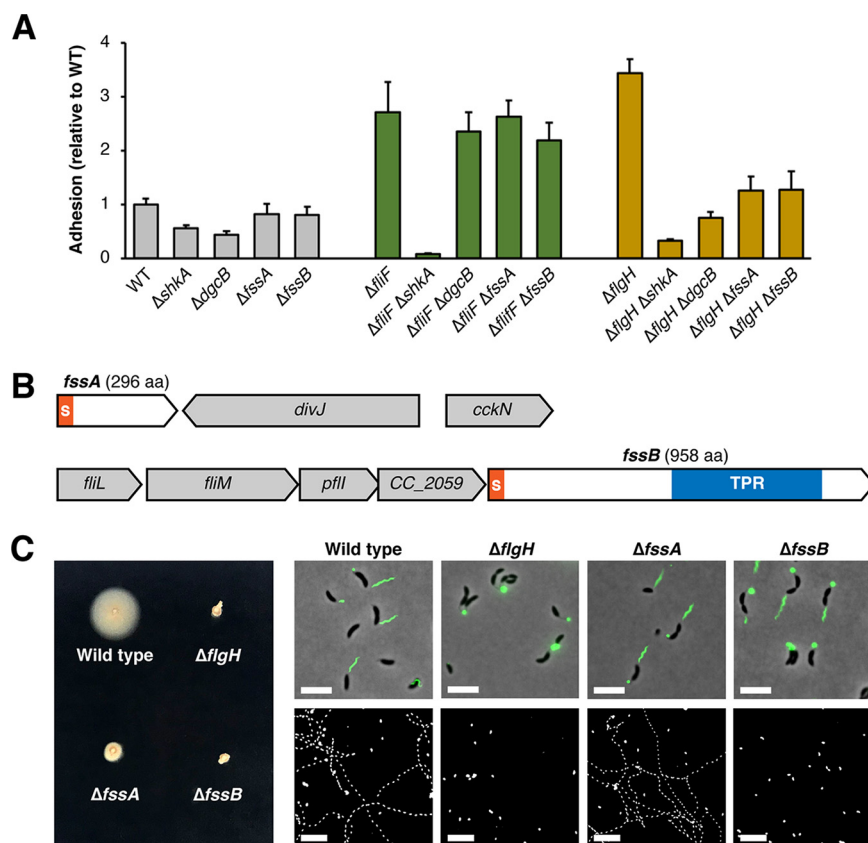
FIG 3 Two novel motility genes contribute to activation of the mechanical pathway. (A) Crystal violet-based attachment assay evaluating suppression of early and late flagellar assembly mutants by individual *fss* genes. Mean values from six biological replicates are shown with error bars representing the associated standard deviations. (B) Genomic context of the *fssA* and *fssB* genes. Orange S, secretion signal; blue bar, tetratricopeptide repeat region. (C) Motility phenotypes of the Δ*fssA* and Δ*fssB* mutants. (Left) Soft agar motility assay. (Top right) Flagellar filaments stained with Alexa-488/maleimide after introduction of the *fljK*[T103C] allele into the indicated mutants. Note that the maleimide dye cross-reacts with holdfast. Scale bars, 5 μm. (Bottom right) Maximum projections from time-lapse microscopy. Cells appear in white, and tracks for motile cells appear as dotted lines. Scale bars, 25 μm.

phenotype in the Δ*flgH* mutant (Fig. 3A), providing evidence that *fssA* and *fssB* contribute to holdfast stimulation through the stator-dependent, mechanical pathway.

New motility factors contribute to mechanical activation. To understand how *fssA* and *fssB* regulate holdfast synthesis, we examined the motility phenotypes of Δ*fssA* and Δ*fssB* deletions. Both mutants were severely impaired in their ability to spread through soft agar. When a flagellin allele (*fljK*[T103C]) coding for an FljK protein that can be stained with maleimide-conjugated dyes (34) was introduced, flagellar filaments were observed in both Δ*fssA* and Δ*fssB* cells. Thus, the motility phenotypes in these mutants are not caused by disruptions to flagellar assembly. Examination of individual cells in liquid broth revealed that Δ*fssB* cells were nonmotile, while some Δ*fssA* cells retained the ability to swim (Fig. 3C). Thus, the Δ*fssB* mutant displays a paralyzed flagellum phenotype analogous to a Δ*motB* mutant, but the motility phenotype in the Δ*fssA* mutant is specific to soft agar.

Over the course of our studies, we observed that the Δ*fssA* mutant had a propensity to begin spreading through soft agar after prolonged incubation on plates (Fig. 4A). Colonies migrated from the inoculation site in an anisotropic manner, suggesting that second-site suppressors of the motility defect had emerged. Indeed, single colonies isolated from motile Δ*fssA* flares were indistinguishable from the wild type when
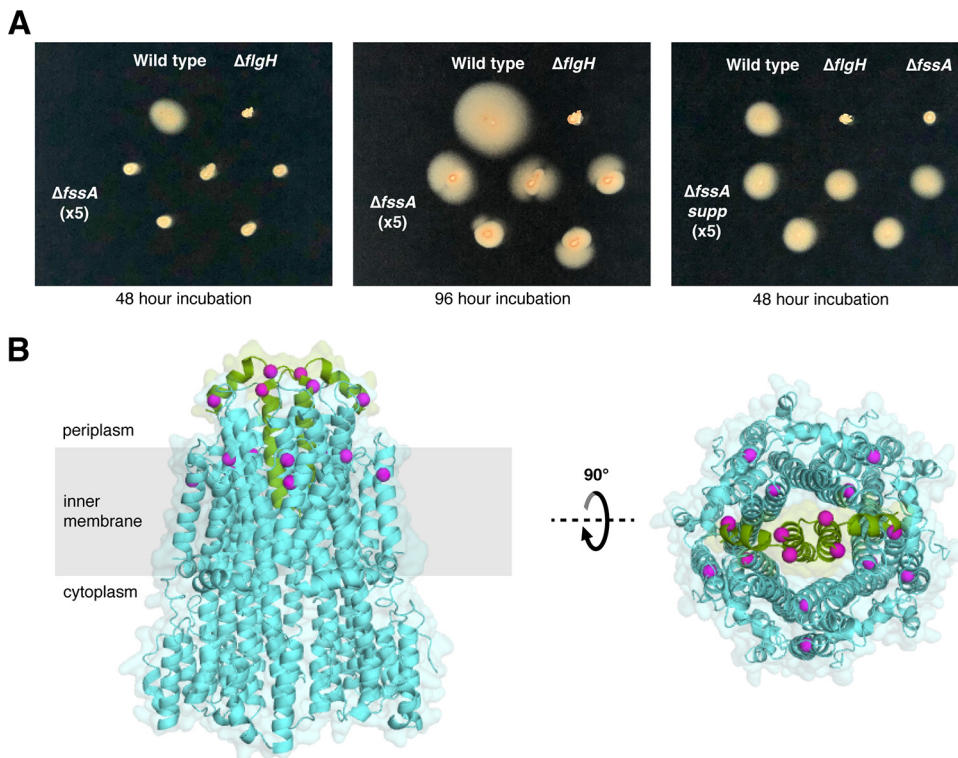
FIG 4 Suppression of the Δ*fssA* motility phenotype by second-site mutations in the stator genes. (A) Soft agar motility assays showing the emergence of motile flares after prolonged incubation of the Δ*fssA* mutant. Single colonies isolated from the leading edge of flares (middle image) displayed wild-type motility when reinoculated into soft-agar (right image). (B) Mapping of Δ*fssA* suppressors onto a homology model of the *C. crescentus* stator. Mutations are located at the periplasmic face of the complex. Identification of multiple mutations in the "plug" region of MotB suggests that the suppressing mutations activate ion translocation ectopically.

reinoculated into soft agar. Fourteen of these motile suppressors were analyzed by whole-genome sequencing to identify the causative mutations. Each isolate harbored a missense mutation in one of the stator genes. Three contained a mutation in *motA*, and 11 contained a mutation in *motB*. Nine of the eleven *motB* mutations disrupt the same residue, serine 52, and six produce the same allele, *motB*^{S52C} (see Fig. S3).

We used a cryoelectron microscopy reconstruction of the MotAB stator from *Campylobacter jejuni* (48) to predict the structure of the *C. crescentus* stator complex. The resulting homology model contains a characteristic transmembrane channel composed of five MotA subunits that is capped at its periplasmic face by two MotB protomers (48, 49). When Δ*fssA* suppressing mutations were mapped onto this model, they displayed a clear bias toward residues on the periplasmic face of the complex (Fig. 4B), with the *motB* mutations all disrupting a region known as the plug. Deleting the plug allows ion translocation through the stators in the absence of productive engagement with a rotor (50), and missense mutations in the plug have been shown to support motility under nonpermissive conditions through gain-of-function activation of the motor (51).

The ability of plug mutations to suppress the Δ*fssA* motility defect indicates that Δ*fssA* and Δ*fssB* mutants display related motility phenotypes. The Δ*fssB* mutant produces an inactive flagellar motor that cannot turn a filament (Fig. 3C), while Δ*fssA* mutant assembles a modestly defective motor that supports full motility in soft agar only when the stators are activated by mutations predicted to increase ion translocation (Fig. 4). A Δ*fssA* Δ*fssB* double mutant did not spread through soft agar even after prolonged incubation, confirming that the lack of motor rotation in Δ*fssB* is epistatic to
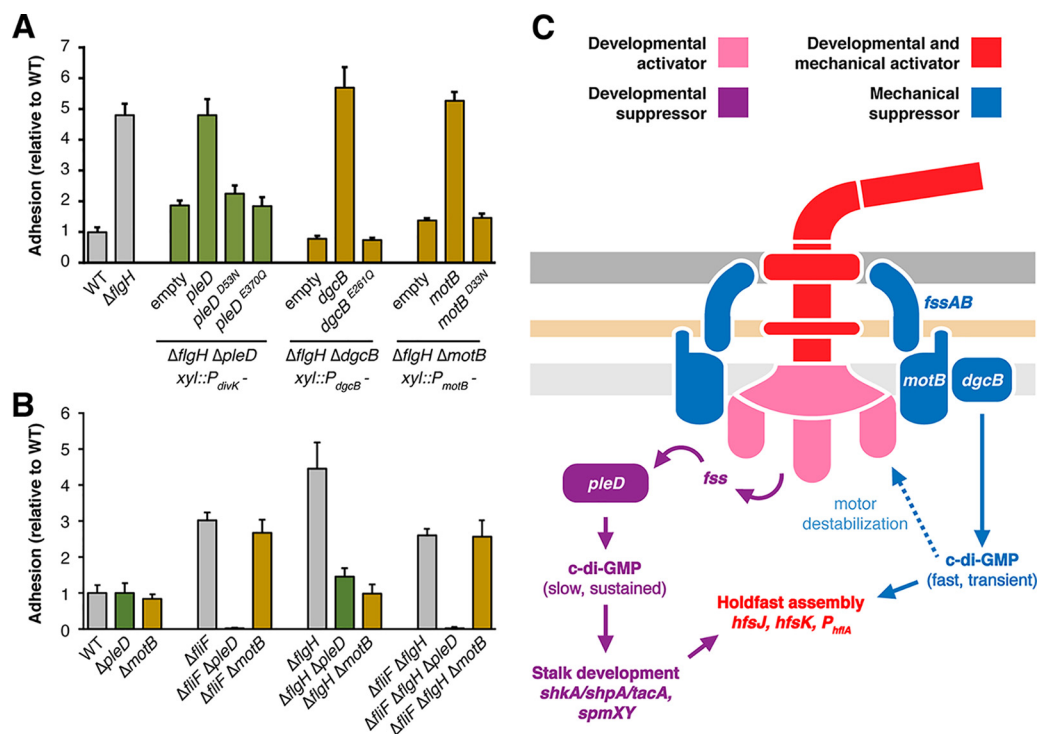
FIG 5 Convergence of flagellar signaling on cyclic-di-GMP. (A) Crystal violet-based attachment assay showing that inactive alleles of *fss* genes in the developmental (*pleD*) and mechanical (*dgcB* and *motB*) pathways do not support flagellar signaling. Each allele is expressed from the gene's native promoter and integrated as a single copy at the *xylX* locus. The genotype and promoter for each strain are indicated below the solid line. Mean values from seven biological replicates are shown with error bars representing the associated standard deviations. (B) Crystal violet-based attachment assay showing that early flagellar mutants are epistatic to late flagellar mutants for activation of the mechanical pathway. The Δ*fliF* Δ*flgH* strain phenocopies the Δ*fliF* strain and demonstrates that the effect of *motB* on adhesion requires early stages of flagellar assembly. Mean values from five biological replicates are shown with the associated standard deviations. (C) Two signaling pathways operate downstream of the flagellum in *C. crescentus*. We propose that mechanical signals are transmitted through the motor to activate DgcB, producing a transient burst of c-di-GMP synthesis that directly activates holdfast biosynthesis enzymes. Persistent filament obstruction activates PleD by destabilizing the motor and triggering flagellar disassembly. PleD activation through this mechanism is predicted to induce sustained c-di-GMP production and initiation of the transcriptional program that leads to stalk development.

the partial defect in Δ*fssA* (see Fig. S3). Furthermore, our data indicate that *fssA* and *fssB* support flagellar signaling by the same the mechanism, since the Δ*fssA* and Δ*fssB* mutations did suppress Δ*flgH* hyperadhesion in an additive manner (see Fig. S3). We conclude that *fssA* and *fssB* are required for proper stator activity in *C. crescentus*. We propose that mutating either gene disrupts both the stator's ability to promote motility and its capacity to transduce mechanical signals.

Separate mechanisms for activating c-di-GMP production. Though the developmental and mechanical pathways can be separated genetically, they ultimately converge to modulate holdfast production. Each pathway includes a diguanylate cyclase predicted to synthesize bis-(3′–5′)-cyclic diguanosine monophosphate (c-di-GMP), a second messenger that promotes surface-associated behaviors in bacteria (52). In *C. crescentus*, c-di-GMP binds numerous downstream effectors to activate stalk assembly (53), cell cycle progression (54, 55), and holdfast synthesis (40, 56). To test the role of c-di-GMP synthesis in linking cues from the flagellum to holdfast production, we examined catalytically inactive alleles of *pleD* and *dgcB*. In contrast to wild-type alleles, *pleD*[E370Q] (57) and *dgcB*[E261Q] (40) failed to restore hyperadhesion in the Δ*flgH* Δ*pleD* and Δ*flgH* Δ*dgcB* backgrounds, respectively, confirming that c-di-GMP synthesis by these enzymes is required to support flagellar signaling through both mechanical and developmental pathways (Fig. 5A).

We examined mechanisms by which the diguanylate cyclase activities of PleD and

DgcB are activated during flagellar signaling. PleD contains a receiver domain at its N terminus that includes a canonical aspartyl phosphorylation site (57, 58). Introducing the nonphosphrylatable $pleD^{D53N}$ allele failed to restore hyperadhesion in the $\Delta flgH$ $\Delta pleD$ background (Fig. 5A). We conclude that phosphorylation of the PleD receiver domain is required for flagellar perturbations to stimulate holdfast production through the developmental pathway. Proton translocation by MotAB stators is used to generate torque for flagellar filament rotation. A $motB$ allele ($motB^{D33N}$) that prevents proton flux through the stator (40, 59) does not support flagellar signaling in the $\Delta flgH$ background (Fig. 5A). We conclude that proton translocation through MotB is required for flagellar perturbations to stimulate holdfast production via the mechanical pathway.

Our data indicate that active proton translocation is required for mechanical stimulation. This model provides a possible explanation for the disparate suppression patterns we observed in early and late flagellar assembly mutants. We predicted that the mechanical pathway is inactive in early flagellar mutants because stator subunits cannot engage with the motor when rotor assembly is incomplete. Indeed, the $\Delta fliF$ mutant was epistatic to the $\Delta flgH$ mutant with respect to suppression by the $\Delta pleD$ and $\Delta motB$ mutations (Fig. 5B). Adhesion in the $\Delta fliF$ $\Delta flgH$ mutant was eliminated when $pleD$ was deleted but remained unchanged when the $\Delta motB$ mutation was introduced, supporting the model that inner membrane rotor assembly is required for activation of the mechanical pathway.

DISCUSSION

Many bacteria alter their behavior after contact with exogenous surfaces, and flagellar motility is a key regulatory determinant of these responses (38, 60–63). However, efforts to dissect contact-dependent signaling pathways have been confounded by contributions from multiple mechanosensors (62, 64), a reliance on noncanonical signaling machinery (9, 40) and the prevalence of transcription-independent responses (7, 65). In this study, we leveraged the hyperadhesive phenotype induced upon mutation of flagellar assembly genes to dissect the genetic basis for adhesion control by the flagellum in *C. crescentus*. We used a high-throughput phenotyping approach to identify mutations that stimulate adhesion and to classify a large group of genes called flagellar signaling suppressors (*fss*) that contribute to increased holdfast production when flagellar assembly is disrupted. The results have clarified important features of how the *C. crescentus* flagellum regulates adhesion and provided a framework for disentangling signaling networks that control bacterial behavior.

Two genes identified in the *fss* screen, *pleD* and *motB*, have been previously shown to link flagellar function to adhesion, but conflicting models were proposed for how these genes regulate holdfast production (34, 40). We showed that *pleD* and *motB* participate in genetically distinct pathways for activating adhesion. *pleD* and its downstream effector *shkA* contribute to increased holdfast production when any stage of flagellar assembly is disrupted. *motB*, the gene for its associated diguanylate cyclase, *dgcB*, and two previously uncharacterized motility genes contribute to adhesion specifically in late flagellar mutants that retain the ability to assemble inner membrane rotors. We conclude that a mechanical pathway and a developmental pathway operate in parallel to link flagellar function to holdfast production.

Strains harboring deletions ($\Delta motB$, $\Delta fssA$, or $\Delta fssB$) or mutant alleles ($motB^{D33N}$) that disrupt motility without affecting filament assembly cannot support activation of the mechanical pathway (Fig. 2A, 3A, and 5A). In addition, early flagellar assembly mutants display epistatic effects on late assembly mutants by eliminating *motB*'s involvement in stimulating adhesion (Fig. 5B). These results suggest that blocking inner membrane rotor (MS- and C-ring) assembly subverts the mechanical pathway by preventing stator engagement and help to explain the range of behavioral effects often observed in flagellar assembly mutants (5, 40, 66). We conclude that intact motors capable of generating torque are required for mechanical activation of the *C. crescentus* flagellum. Increased load on rotating filaments leads to the recruitment of additional

stators to the motor in enteric bacteria (67, 68), and a similar resistance sensing mechanism likely supports tactile sensing in *C. crescentus*. Mutants in mechanical pathway genes such as *fssA* and *fssB* should prove useful in describing the structural basis for how such changes in load are sensed by the flagellar motor.

Key features of the mechanical pathway mirror the tactile sensing event described by Hug et al. (40), but certain conclusions must be reevaluated in light of our results. We showed that late flagellar mutants display increased holdfast production in M2X liquid medium (Fig. 2C; see also Fig. S1) in the absence of a surface and under nutrient conditions for which tactile sensing does not normally occur (34). We conclude that mutants lacking the outer parts of the flagellum do not show a hypersensitive surface response. Instead, we infer that the motor responds to the absence of a filament as it would to an obstructed filament by activating stator-dependent signaling ectopically. Consistent with this interpretation, preventing stators from productively engaging with the rotor, either by disrupting proteins required for stator function (Fig. 2A and 3A) or by mutating early flagellar genes that code for rotor components, blocks mechanical signaling in late assembly mutants (Fig. 5B). This explains the perplexing epistasis of inner parts of the flagellum over outer parts (69) and supports established models for tactile sensing through increased load on the filament (60) rather than the motor acting as a tetherless sensor (40). More broadly, the disparate phenotypes identified here for stator, rotor, and hook-basal body mutants reflect an emerging pattern seen in other organisms and argue that signal bifurcation by the flagellum is a conserved feature throughout bacteria (70, 71).

The identification of a second, developmental pathway downstream of the flagellum is consistent with previous studies showing that late flagellar assembly mutants display contact-independent increases in holdfast production (33, 34). In fact, disrupting flagellar assembly at any stage stimulates adhesion (Fig. 2A), and our analysis of this process highlights an overlooked role for the flagellum in controlling the *C. crescentus* developmental program. We explicitly characterized *pleD* and *shkA*, but other developmental regulators identified in the *fss* screen (*shpA*, *tacA* [47], *spmX* [72], *spmY* [73], *zitP*, *cpaM* [74], *sciP* [75], and *rpoN* [76]) likely also act downstream of both early and late flagellar mutants to stimulate adhesion. Most of these genes influence flagellar assembly either directly or by altering cell cycle progression. For instance, *pleD* promotes flagellar disassembly by stimulating proteolytic turnover of the MS-ring protein FliF (77), but our results indicate that PleD is also stimulated through phosphorylation at D53 when flagellar assembly is disrupted (Fig. 4A). Thus, cell cycle regulators that control flagellar assembly simultaneously act downstream of the flagellum in regulating holdfast production. This duality raises the intriguing possibility that specific environmental cues activate flagellar disassembly as part of a positive-feedback loop that reinforces the commitment to differentiate into a stalked cell.

The developmental and mechanical pathways we identified each require a distinct diguanylate cyclase, suggesting that flagellar signaling converges to stimulate adhesion by modulating c-di-GMP levels (Fig. 4C). Signaling through the mechanical pathway requires stator subunits that can productively engage with the rotor, and we propose that increased load on the flagellar filament induces conformational changes in the motor that activate the stator-associated diguanylate cyclase DgcB. This mechanism differs from contact-dependent activation of c-di-GMP synthesis by SadC in *Pseudomonas aeruginosa*, which requires disengagement of the MotCD stator (78). *P. aeruginosa* uses a MotAB stator system for swimming in liquid and a second, MotCD stator for swarming on surfaces (79). Thus, the signaling competency of engaged stators in *C. crescentus* could be an intrinsic feature of single-stator systems. Separately, c-di-GMP synthesis by PleD is part of a multitiered system controlling the master cell cycle regulator CtrA in *C. crescentus* (53, 80), and we provided evidence that the status of flagellar assembly feeds into this developmental program by regulating PleD phosphorylation (Fig. 5A). Whether the flagellum controls PleD phosphorylation through the DivJ-PleC kinase-phosphatase pair (57) or through a separate phosphorelay will

require additional dissection of how *fss* genes link flagellar assembly to cell cycle progression.

Despite the apparent convergence of flagellar signaling on two diguanylate cyclases, *pleD* and *dgcB* stimulate holdfast production by different mechanisms. When the mechanical pathway is bypassed by disrupting early stages of flagellar assembly, *shkA* and *pleD* are required for holdfast production, but *dgcB* is dispensable (Fig. 2A and 3A). ShkA is a histidine kinase that is stimulated by c-di-GMP (81). It initiates a phosphotransfer that activates the transcriptional coactivator TacA, upregulating dozens of genes required for stalk biogenesis (47). A requirement for both *pleD* and *shkA* in the developmental pathway indicates that *pleD* controls holdfast production specifically through the *tacA* transcriptional program. In contrast, the *dgcB*-dependent c-di-GMP pool has been shown to act through direct activation of holdfast synthesis enzymes (40). Thus, PleD and DgcB likely act on different timescales, and we favor a model in which the sequential accumulation of c-di-GMP drives the transition to permanent attachment. In this scenario, increased load on the flagellar filament would activate DgcB, producing a transient burst of c-di-GMP that immediately stimulates holdfast production. Persistent filament obstruction would increase c-di-GMP levels sufficiently to destabilize the motor, leading to flagellar disassembly, activation of sustained c-di-GMP synthesis by PleD and the onset of stalked cell development (Fig. 5C).

Using an unbiased screen to identify flagellar signaling genes has allowed us to propose a unified model for the mechanism by which the flagellum regulates holdfast production in *C. crescentus*. Intact flagellar motors respond to assembly defects in their associated filaments (Fig. 2A and 5B), but perturbing the flagellum also influences the timing of holdfast production by altering cell cycle signaling (34) (Fig. 2A and 5A). Candidate approaches specifically targeting developmental or tactile sensing phenomena have not accounted for presence of multiple pathways downstream of the flagellum. Though two pathways can be distinguished genetically in flagellar mutants, overlap between developmental, mechanical, and other signaling pathways during actual surface encounters has likely confounded interpretations of how the flagellum regulates holdfast production. The complexity of these circuits underscores how bacterial behavior is not controlled by linear signaling pathways. Flagellar cues represent only a subset of the stimuli known to influence adhesion. Nutrient availability, redox homeostasis, chemotaxis, and T4P dynamics all influence whether *C. crescentus* produces a holdfast. Disentangling how diverse signaling networks converge to regulate holdfast production has the power to illuminate how environmental information is integrated to control behavior.

MATERIALS AND METHODS

Bacterial growth and genetic manipulation. Strains and plasmids used in this study are listed in Tables S4 and S5 in the supplemental material. Standard PCR and Gibson assembly (82) methods were used for developing plasmid constructs. Strains, plasmids, primer sequences, and details of construction are available upon request. *Escherichia coli* cultures were grown in Luria-Bertani (LB) medium at 37°C supplemented with 1.5% (wt/vol) agar and 50 μg/ml kanamycin when necessary. Unless otherwise noted, *C. crescentus* cultures were grown at 30°C in peptone-yeast extract (PYE) medium supplemented with 1.5% (wt/vol) agar, 3% (wt/vol) sucrose, and 25 μg/ml kanamycin when necessary or in M2 defined medium supplemented with 0.15% (wt/vol) xylose (83). Plasmids were introduced into *C. crescentus* by electroporation. Unmarked deletions were constructed using *sacB*-based counterselection in sucrose as described previously (33).

Genetic complementation of mutants. Mutants were complemented by genomic integration of the appropriate gene as a single copy at a neutral site (*xylX*) and under the gene's native promoter. Specifically, predicted open reading frames were fused to their predicted promoter sequences and inserted into the NdeI/SacI site of pMT585 (pXGFPC-2) (84). Each promoter-gene cassette was inserted in reverse orientation to allow for transcription in the opposite direction relative to the *xylX* promoter upstream of the cloning site. Surface attachment and motility assays used to evaluate complementation are described below (see Fig. S4).

Tn-*Himar* mutant library construction and mapping. Construction and mapping of the two barcoded transposon libraries was performed based on the procedure developed by Wetmore et al., as described previously (33, 85). Cells from 25-ml cultures of the APA_752 barcoded transposon pool that had been grown to mid-log phase in LB medium supplemented with kanamycin and 300 μM diaminopimelic acid (DAP) and 25 ml of either the *C. crescentus* CB15 wild-type or the Δ*flgH* mutant strain that had

been grown to mid-log phase in PYE were collected by centrifugation, washed twice with PYE containing 300 μM DAP, mixed, and spotted together on a PYE agar plate containing 300 μM DAP. After the plate was incubated overnight at room temperature, the cells were scraped from the plate, resuspended in PYE medium, and spread onto 20 150-mm PYE agar plates containing kanamycin, followed by incubation at 30°C for 3 days. Colonies from each plate were scraped into PYE medium and used to inoculate a 25-ml PYE culture containing 5 μg/ml kanamycin. The culture was grown for three doublings, glycerol was added to 20%, and 1-ml aliquots were frozen at −80°C.

Library mapping was performed as described previously (85). Briefly, genomic DNA was isolated from three 1-ml aliquots of each library. The DNA was sheared, and ~300-bp fragments were selected before end repair. A Y-adapter (Mod2_TS_Univ, Mod2_TruSeq) was ligated and used as a template for transposon junction amplification with the primers Nspacer_BarSeq_pHIMAR and either P7_mod_TS_index1 or P7_mod_TS_index2. Then, 150-bp single-end reads were collected on an Illumina HiSeq 2500 in rapid-run mode, and the genomic insertion positions were mapped and correlated with a unique barcode using BLAT (86) and MapTnSeq.pl to generate a mapping file with DesignRandomPool.pl. All code is available at https://bitbucket.org/berkeleylab/feba/. Features of the barcoded transposon libraries can be found in Table S6.

Adhesion profiling of barcoded Tn-*Himar* mutant libraries. Adhesion profiling was performed as described by Hershey et al. (33), with slight modifications. Cells from 1-ml aliquots of each barcoded transposon library were collected by centrifugation and resuspended in 1 ml of M2X medium, and 300 μl was inoculated into a well of a 12-well microtiter plate containing 1.5 ml of M2X medium with six to eight approximately 1×1-cm layers of cheesecloth. Microtiter plates containing selections were grown for 24 h at 30°C with shaking at 155 rpm, and then 150 μl of the culture was passaged by inoculation into a well with 1.65 ml of fresh M2X-containing cheesecloth. Cells from an additional 500 μl of depleted medium were harvested by centrifugation and stored at −20°C for BarSeq analysis. Each passaging experiment was performed in triplicate, and passaging was performed sequentially for a total of five rounds of selection. Identical cultures grown in a plate without cheesecloth were used as a nonselective reference condition.

Cell pellets were used as PCR templates to amplify the barcodes in each sample using indexed primers (85). Amplified products were purified and pooled for multiplexed sequencing. Next, 50-bp single-end reads were collected on an Illumina HiSeq4000. MultiCodes.pl, combineBarSeq.pl, and FEBA.R were used to determine fitness by comparing the log$_2$ ratios of barcode counts in each sample over the counts from a nonselective growth in M2X without cheesecloth. To evaluate mutant phenotypes in each screen, the replicates were used to calculate a mean fitness score for each gene after each passage. The mean fitness was summed across passages for each gene and ranked by either the lowest (wild-type background) or highest (Δ*flgH* background) summed fitness score.

Surface attachment measurement by crystal violet staining. Overnight *C. crescentus* cultures grown in PYE were diluted to an optical density at 660 nm (OD$_{660}$) of 0.5 with PYE, and 1.5 μl from each diluted starter culture was inoculated into the wells of a 48-well microtiter plate containing 450 μl of M2X medium. The number of replicates for each experiment ranged from 5 to 8 and is indicated in the relevant figure legend. Plates were grown at 30°C with shaking at 155 rpm for 17 h; the cultures were then discarded, and the wells were washed thoroughly under a stream of tap water. Attached cells were stained by adding 500 μl of an aqueous solution containing 0.01% (wt/vol) crystal violet to each well and shaking the plates for 5 min. Excess dye was discarded, the wells were again washed under a stream of tap water, and the remaining dye was dissolved by adding 500 μl of ethanol to each well. Staining was quantified by reading the absorbance at 575 nm using a Tecan Spark microplate reader. Each reading was corrected by subtracting the absorbance value for an uninoculated medium blank; the mean of the biological replicates for each strain was calculated and normalized to the mean value measured for the wild-type background. To minimize day-to-day variation in the absolute CV staining values, each figure panel shows an internally controlled experiment with all measurements taken from the same plate on the same day. The collection of strains shown in each figure was assayed together on at least four independent days, and a representative data set is shown.

Holdfast staining with fluorescent wheat germ agglutinin. Next, 2 ml of M2X medium was inoculated to achieve a starting OD$_{660}$ of 0.001 using saturated starter cultures grown in PYE. After growth to an OD$_{660}$ of 0.07 to 0.1, 400 μl of each culture was added to a fresh 1.5-ml Eppendorf tube containing 1 μl of a 2 mg/ml solution of WGA conjugated with Alexa-594. After a 5-min incubation at room temperature in the dark, the cells were harvested at 6,000 × *g*, washed with distilled water, and resuspended in the residual liquid after centrifugation. Then, 1 μl was spotted onto a glass slide, and a cover slip was placed on top. Imaging was performed with a Leica DM5000 microscope equipped with an HCX PL APO63X/1.4-numerical-aperture Ph3 objective. A red fluorescent protein filter (Chroma set 41043) was used to visualize wheat germ agglutinin (WGA) foci. Cells with a holdfast were counted manually on five separate days. A minimum of 95 cells were counted for each biological replicate.

For direct staining of liquid cultures without centrifugation, cells were grown as described above. Next, 400 μl was removed and imaged using the standard protocol described above, and 0.8 μl from a 2-mg/ml fWGA solution was added directly to the remaining culture. Cultures were shaken with the dye for 5 min in the dark, and 1.5 μl was spotted onto a microscope slide, covered, and imaged immediately as described above.

Analysis of holdfast polysaccharide in spent medium. Holdfast release was analyzed as described previously (43). Cultures (10 ml) grown for 24 h in M2X were centrifuged at 7,000 × *g* for 10 min. A 2-ml portion of supernatant (spent medium) was moved to a fresh tube, 3 ml of 100% ethanol was added, and the mixture was incubated overnight at 4°C. Precipitate was isolated by centrifugation for 1 h at

18,000 × *g* and suspended in 50 μl of TU buffer (10 mM Tris-HCl [pH 8.2], 4 M urea). Twofold serial dilutions were prepared, and 3 μl of each dilution was spotted on nitrocellulose to absorb for 20 min. The membrane was then blocked overnight with 5% bovine serum albumin (BSA) dissolved in TBST buffer (20 mM Tris-HCl [pH 8.0], 137 mM NaCl, 2.7 mM KCl, 0.1% Tween 20), followed by a 1-h incubation with 5% BSA in TBST containing 1.5 μg/ml fWGA. The membrane was washed with TBST and imaged with a Bio-Rad ChemiDoc imager using the Alexa Fluor-647 setting.

Soft-agar motility assay. Overnight cultures grown in PYE were diluted to an OD_{660} of 0.5, and 1.5 μl was pipetted into a PYE plate containing 0.3% agar. Plates were sealed with parafilm, incubated for 72 h at 30°C, and photographed.

Flagellar filament staining. Next, 2 ml of PYE medium was inoculated to a starting OD_{660} of 0.05 using saturated overnight starter cultures and grown at 30°C to mid-log phase (OD_{660} = 0.3 to 0.4). Portions (500 μl) of each culture were mixed with 0.5 μl of a 2-mg/ml solution of Alexa-488/maleimide in dimethyl sulfoxide, followed by incubation for 10 min in the dark. Cells were harvested by centrifugation at 6,000 × *g* for 1.5 min, washed with 500 μl of PYE, recentrifuged, and suspended in 500 μl of PYE. Then, 1 μl of the stained cell suspension was spotted onto a pad of PYE solidified with 1% agarose. Imaging was performed as described above but with the use of a green fluorescent protein filter (Chroma set 41017) for flagellin visualization. Note that Alexa-488/maleimide cross-reacts with the holdfast.

Microscopic analysis of swimming behavior. Then, 2 ml of PYE was inoculated to an OD_{660} of 0.1 with saturated overnight starters and grown at 30°C to an OD_{660} of 0.4 to 0.5. A 2.69% (wt/vol) solution of 2.0-μm polystyrene spacer beads (Polysciences) was diluted 1,000-fold in 1 ml of PYE. Equal volumes of liquid culture and diluted spacer beads were mixed and spotted onto a slide. Dark-field images were collected at 100-ms intervals for 30 s using a Leica 40× PH2 objective. Maximum projections from each time series are presented.

Mapping of Δ*fssA* suppressor mutations. To isolate motile suppressors, 1.5 μl from a saturated Δ*fssA* culture grown in PYE was spotted onto PYE plates containing 0.3% agar. Plates were sealed and incubated for 96 h at 30°C. Cells from the leading edge of spreading flares (Fig. 4A) were streaked onto a standard PYE plate, and the plates were incubated at 30°C for 72 h. A single colony was inoculated into PYE broth and grown to saturation. To avoid isolating siblings, only one suppressor was isolated from each initial soft-agar spotting. Genomic DNA from 14 suppressors, as well as the original Δ*fssA* parent background, was isolated as described above. Libraries were prepared based on the Illumina Nextera protocol, and single-end reads were collected using the NextSeq 550 platform at the Microbial Genome Sequencing Center (MiGS, Pittsburgh, PA). Mutations were identified using breseq (87) with the *C. crescentus* NA1000 as a reference genome (GenBank accession no. CP001340).

Homology modeling of *Cc*MotAB. To develop a structural model of the *C. crescentus* stator, we used the MotA and MotB protein sequences (accession numbers CCNA_00787 and CCNA_01644) to search a protein structure fold library using the HHpred/HHSearch package for homology detection (88) within the Phyre2 pipeline (89). For *C. crescentus* MotB, this approach yielded high confidence (>99%) structural models of the N- and C-terminal halves of the protein that aligned to multiple published MotB structures, including the N terminus of *C. jejuni* MotB (PDB ID 6YKM). The *C. crescentus* MotA model aligned to the entire length of *Campylobacter jejuni* MotA (PDB ID 6YKM) with high confidence (100%). The coordinates of the *Cc*MotA and N-terminal *Cc*MotB homology models were used to build a 5:2 MotA:MotB complex by aligning them to the 6YKM *C. jejuni* MotAB model.

β-**Galactosidase assay.** Strains carrying a P_{hfiA}-*lacZ* transcriptional reporter (35) were inoculated from colonies on PYE-agar plates into 2 ml of M2X medium and grown shaking at 200 rpm overnight at 30°C. Overnight cultures were diluted in 2 ml of fresh M2X to an OD_{660} of 0.05 and grown for ~6 h to the early exponential phase. These cultures were then diluted again into 2 ml of fresh M2X to an OD_{660} of 0.001 and grown for 17 h to a final OD_{660} of 0.1. The *β*-galactosidase activity was then was measured colorimetrically, as previously described (35). Briefly, 0.15-ml portions of cells were permeabilized by vortexing with 50 μl of chloroform and 50 μl of PYE broth as an emulsifier. Then, 600 μl of Z-buffer (60 mM Na_2HPO_4, 40 mM NaH_2PO_4, 10 mM KCl, 1 mM $MgSO_4$) was added, followed by 200 μl ONPG (o-nitrophenyl-*β*-D-galactopyranoside) in 0.1 M KPO_4. After 5 min at room temperature, reactions were quenched with 1 ml of 1 M Na_2CO_3, and absorbance at 420 nm was used to calculate the *β*-galactosidase activity.

Data availability. Sequence data have been deposited in the NCBI Sequence Read Archive (SRA) under the following project accession numbers. For wild-type *C. crescentus*, PRJNA640825 contains the sequence data used to map the barcoded Tn-*Himar* library, and PRJNA640525 contains barcoded amplicon sequences collected after passaging in cheesecloth. For the Δ*flgH* mutant, PRJNA640725 contains the sequencing data used to map the barcoded Tn-*Himar* library, and PRJNA641033 contains barcoded amplicon sequences collected after passaging in cheesecloth. PRJNA672134 contains whole-genome sequencing data for the Δ*fssA* parent strain and 14 motile suppressors.

SUPPLEMENTAL MATERIAL

Supplemental material is available online only.

FIG S1, JPG file, 0.5 MB.

FIG S2, JPG file, 0.3 MB.

FIG S3, JPG file, 0.5 MB.

FIG S4, JPG file, 1.5 MB.

TABLE S1, XLSX file, 0.01 MB.
TABLE S2, XLSX file, 0.01 MB.
TABLE S3, XLSX file, 0.01 MB.
TABLE S4, XLSX file, 0.01 MB.
TABLE S5, XLSX file, 0.01 MB.
TABLE S6, XLSX file, 0.01 MB.

REFERENCES

1. Zobell CE. 1943. The effect of solid surfaces upon bacterial activity. J Bacteriol 46:39–56. https://doi.org/10.1128/JB.46.1.39-56.1943.
2. Donlan RM. 2002. Biofilms: microbial life on surfaces. Emerg Infect Dis 8:881–890. https://doi.org/10.3201/eid0809.020063.
3. Chavez-Dozal A, Gorman C, Erken M, Steinberg PD, McDougald D, Nishiguchi MK. 2013. Predation response of *Vibrio fischeri* biofilms to bacterivorus protists. Appl Environ Microbiol 79:553–558. https://doi.org/10.1128/AEM.02710-12.
4. Berne C, Ellison CK, Ducret A, Brun YV. 2018. Bacterial adhesion at the single-cell level. Nat Rev Microbiol 16:616–627. https://doi.org/10.1038/s41579-018-0057-5.
5. McCarter L, Hilmen M, Silverman M. 1988. Flagellar dynamometer controls swarmer cell differentiation of *V. parahaemolyticus*. Cell 54:345–351. https://doi.org/10.1016/0092-8674(88)90197-3.
6. Watnick PI, Kolter R. 1999. Steps in the development of a *Vibrio cholerae* El Tor biofilm. Mol Microbiol 34:586–595. https://doi.org/10.1046/j.1365-2958.1999.01624.x.
7. Levi A, Jenal U. 2006. Holdfast formation in motile swarmer cells optimizes surface attachment during *Caulobacter crescentus* development. J Bacteriol 188:5315–5318. https://doi.org/10.1128/JB.01725-05.
8. Mueller RS, McDougald D, Cusumano D, Sodhi N, Kjelleberg S, Azam F, Bartlett DH. 2007. *Vibrio cholerae* strains possess multiple strategies for abiotic and biotic surface colonization. J Bacteriol 189:5348–5360. https://doi.org/10.1128/JB.01867-06.
9. Petrova OE, Sauer K. 2011. SagS contributes to the motile-sessile switch and acts in concert with BfiSR to enable *Pseudomonas aeruginosa* biofilm formation. J Bacteriol 193:6614–6628. https://doi.org/10.1128/JB.00305-11.
10. Collier J. 2016. Cell cycle control in *Alphaproteobacteria*. Curr Opin Microbiol 30:107–113. https://doi.org/10.1016/j.mib.2016.01.010.
11. Haiko J, Westerlund-Wikström B. 2013. The role of the bacterial flagellum in adhesion and virulence. Biology (Basel) 2:1242–1267. https://doi.org/10.3390/biology2041242.
12. Belas R. 2014. Biofilms, flagella, and mechanosensing of surfaces by bacteria. Trends Microbiol 22:517–527. https://doi.org/10.1016/j.tim.2014.05.002.
13. Aldridge P, Hughes KT. 2002. Regulation of flagellar assembly. Curr Opin Microbiol 5:160–165. https://doi.org/10.1016/s1369-5274(02)00302-8.
14. Ramakrishnan G, Zhao JL, Newton A. 1994. Multiple structural proteins are required for both transcriptional activation and negative autoregulation of *Caulobacter crescentus* flagellar genes. J Bacteriol 176:7587–7600. https://doi.org/10.1128/jb.176.24.7587-7600.1994.
15. Stephens C, Mohr C, Boyd C, Maddock J, Gober J, Shapiro L. 1997. Identification of the *fliI* and *fliJ* components of the *Caulobacter flagellar* type III protein secretion system. J Bacteriol 179:5355–5365. https://doi.org/10.1128/jb.179.17.5355-5365.1997.
16. Ohta N, Chen L-S, Swanson E, Newton A. 1985. Transcriptional regulation of a periodically controlled flagellar gene operon in *Caulobacter crescentus*. J Mol Biol 186:107–115. https://doi.org/10.1016/0022-2836(85)90261-x.
17. Jenal U. 2000. Signal transduction mechanisms in *Caulobacter crescentus* development and cell cycle control. FEMS Microbiol Rev 24:177–191. https://doi.org/10.1016/S0168-6445(99)00035-2.
18. Khan S, Dapice M, Reese TS. 1988. Effects of *mot* gene expression on the

structure of the flagellar motor. J Mol Biol 202:575–584. https://doi.org/10.1016/0022-2836(88)90287-2.
19. Blair DF, Berg HC. 1990. The MotA protein of *Escherichia coli* is a proton-conducting component of the flagellar motor. Cell 60:439–449. https://doi.org/10.1016/0092-8674(90)90595-6.
20. Henrichsen J. 1972. Bacterial surface translocation: a survey and a classification. Bacteriol Rev 36:478–503. https://doi.org/10.1128/MMBR.36.4.478-503.1972.
21. Schneider WR, Doetsch RN. 1974. Effect of viscosity on bacterial motility. J Bacteriol 117:696–701. https://doi.org/10.1128/JB.117.2.696-701.1974.
22. Berg HC, Tedesco PM. 1975. Transient response to chemotactic stimuli in *Escherichia coli*. Proc Natl Acad Sci U S A 72:3235–3239. https://doi.org/10.1073/pnas.72.8.3235.
23. Wadhwa N, Phillips R, Berg HC. 2019. Torque-dependent remodeling of the bacterial flagellar motor. Proc Natl Acad Sci U S A 116:11764–11769.
24. Pratt LA, Kolter R. 1998. Genetic analysis of *Escherichia coli* biofilm formation: roles of flagella, motility, chemotaxis, and type I pili. Mol Microbiol 30:285–293. https://doi.org/10.1046/j.1365-2958.1998.01061.x.
25. O'Toole GA, Kolter R. 1998. Flagellar and twitching motility are necessary for *Pseudomonas aeruginosa* biofilm development. Mol Microbiol 30:295–304. https://doi.org/10.1046/j.1365-2958.1998.01062.x.
26. Bodenmiller D, Toh E, Brun YV. 2004. Development of surface adhesion in *Caulobacter crescentus*. J Bacteriol 186:1438–1447. https://doi.org/10.1128/jb.186.5.1438-1447.2004.
27. Lauga E. 2016. Bacterial hydrodynamics. Annu Rev Fluid Mech 48:105–130. https://doi.org/10.1146/annurev-fluid-122414-034606.
28. Shapiro L, Agabian-Keshishian N, Bendis I. 1971. Bacterial differentiation. Science 173:884–892. https://doi.org/10.1126/science.173.4000.884.
29. Poindexter JS. 1964. Biological properties and classification of the *Caulobacter* group. Bacteriol Rev 28:231–295. https://doi.org/10.1128/BR.28.3.231-295.1964.
30. Degnen ST, Newton A. 1972. Chromosome replication during development in *Caulobacter crescentus*. J Mol Biol 64:671–680. https://doi.org/10.1016/0022-2836(72)90090-3.
31. Schmidt JM, Stanier RY. 1966. The development of cellular stalks in bacteria. J Cell Biol 28:423–436. https://doi.org/10.1083/jcb.28.3.423.
32. Poindexter JS. 1981. The caulobacters: ubiquitous unusual bacteria. Microbiol Rev 45:123–179. https://doi.org/10.1128/MR.45.1.123-179.1981.
33. Hershey DM, Fiebig A, Crosson S. 2019. A genome-wide analysis of adhesion in *Caulobacter crescentus* identifies new regulatory and biosynthetic components for holdfast assembly. mBio 10:e02273-18. https://doi.org/10.1128/mBio.02273-18.
34. Berne C, Ellison CK, Agarwal R, Severin GB, Fiebig A, Morton IIRI, Waters CM, Brun YV. 2018. Feedback regulation of *Caulobacter crescentus* holdfast synthesis by flagellum assembly via the holdfast inhibitor HfiA. Mol Microbiol 110:219–238. https://doi.org/10.1111/mmi.14099.
35. Fiebig A, Herrou J, Fumeaux C, Radhakrishnan SK, Viollier PH, Crosson S. 2014. A cell cycle and nutritional checkpoint controlling bacterial surface adhesion. PLoS Genet 10:e1004101-14. https://doi.org/10.1371/journal.pgen.1004101.
36. Purcell EB, Siegal-Gaskins D, Rawling DC, Fiebig A, Crosson S. 2007. A photosensory two-component system regulates bacterial cell attachment.

Proc Natl Acad Sci U S A 104:18241–18246. https://doi.org/10.1073/pnas
.0705887104.

37. Reyes Ruiz LM, Fiebig A, Crosson S. 2019. Regulation of bacterial surface attachment by a network of sensory transduction proteins. PLoS Genet 15:e1008022. https://doi.org/10.1371/journal.pgen.1008022.

38. Li G, Brown PJB, Tang JX, Xu J, Quardokus EM, Fuqua C, Brun YV. 2012. Surface contact stimulates the just-in-time deployment of bacterial adhesins. Mol Microbiol 83:41–51. https://doi.org/10.1111/j.1365-2958.2011 .07909.x.

39. Ellison CK, Kan J, Dillard RS, Kysela DT, Ducret A, Berne C, Hampton CM, Ke Z, Wright ER, Biais N, Dalia AB, Brun YV. 2017. Obstruction of pilus retraction stimulates bacterial surface sensing. Science 358:535–538. https://doi.org/10.1126/science.aan5706.

40. Hug I, Deshpande S, Sprecher KS, Pfohl T, Jenal U. 2017. Second messenger–mediated tactile response by a bacterial rotary motor. Science 358:531–534. https://doi.org/10.1126/science.aan5353.

41. Sangermani M, Hug I, Sauter N, Pfohl T, Jenal U. 2019. Tad pili play a dynamic role in Caulobacter crescentus surface colonization. mBio 10: e01237-19. https://doi.org/10.1128/mBio.01237-19.

42. Dingwall A, Gober JW, Shapiro L. 1990. Identification of a Caulobacter basal body structural gene and a cis-acting site required for activation of transcription. J Bacteriol 172:6066–6076. https://doi.org/10.1128/jb.172 .10.6066-6076.1990.

43. Hershey DM, Porfírio S, Black I, Jaehrig B, Heiss C, Azadi P, Fiebig A, Crosson S. 2019. Composition of the holdfast polysaccharide from Caulobacter crescentus. J Bacteriol 201:277–283. https://doi.org/10.1128/JB .00276-19.

44. Paul R, Weiser S, Amiot NC, Chan C, Schirmer T, Giese B, Jenal U. 2004. Cell cycle-dependent dynamic localization of a bacterial response regulator with a novel di-guanylate cyclase output domain. Genes Dev 18:715–727. https://doi.org/10.1101/gad.289504.

45. Leclerc G, Wang SP, Ely B. 1998. A new class of Caulobacter crescentus flagellar genes. J Bacteriol 180:5010–5019. https://doi.org/10.1128/JB.180.19 .5010-5019.1998.

46. Ellison CK, Rusch DB, Brun YV. 2019. Flagellar mutants have reduced pilus synthesis in Caulobacter crescentus. J Bacteriol 201:e00031-19. https://doi .org/10.1128/JB.00031-19.

47. Biondi EG, Skerker JM, Arif M, Prasol MS, Perchuk BS, Laub MT. 2006. A phosphorelay system controls stalk biogenesis during cell cycle progression in Caulobacter crescentus. Mol Microbiol 59:386–401. https://doi.org/ 10.1111/j.1365-2958.2005.04970.x.

48. Santiveri M, Roa-Eguiara A, Kühne C, Wadhwa N, Hu H, Berg HC, Erhardt M, Taylor NMI. 2020. Structure and function of stator units of the bacterial flagellar motor. Cell 183:244–257. https://doi.org/10.1016/j.cell.2020.08 .016.

49. Deme JC, Johnson S, Vickery O, Aron A, Monkhouse H, Griffiths T, James RH, Berks BC, Coulton JW, Stansfeld PJ, Lea SM. 2020. Structures of the stator complex that drives rotation of the bacterial flagellum. Nat Microbiol 5:1553–1564. https://doi.org/10.1038/s41564-020-0788-8.

50. Hosking ER, Vogt C, Bakker EP, Manson MD. 2006. The Escherichia coli MotAB proton channel unplugged. J Mol Biol 364:921–937. https://doi .org/10.1016/j.jmb.2006.09.035.

51. Brenzinger S, Dewenter L, Delalez NJ, Leicht O, Berndt V, Paulick A, Berry RM, Thanbichler M, Armitage JP, Maier B, Thormann KM. 2016. Mutations targeting the plug-domain of the S hewanella oneidensis proton-driven stator allow swimming at increased viscosity and under anaerobic conditions: MotB plug-domain mutants. Mol Microbiol 102:925–938. https:// doi.org/10.1111/mmi.13499.

52. Wolfe AJ, Visick KL. 2008. Get the message out: cyclic-di-GMP regulates multiple levels of flagellum-based motility. J Bacteriol 190:463–475. https://doi.org/10.1128/JB.01418-07.

53. Kaczmarczyk A, Hempel AM, Arx C, Böhm R, Dubey BN, Nesper J, Schirmer T, Hiller S, Jenal U. 2020. Precise timing of transcription by c-di-GMP coordinates cell cycle and morphogenesis in Caulobacter. Nat Commun 11:1–16. https://doi.org/10.1038/s41467-020-14585-6.

54. Duerig A, Abel S, Folcher M, Nicollier M, Schwede T, Amiot N, Giese B, Jenal U. 2009. Second messenger-mediated spatiotemporal control of protein degradation regulates bacterial cell cycle progression. Genes Dev 23:93–104. https://doi.org/10.1101/gad.502409.

55. Lori C, Ozaki S, Steiner S, Böhm R, Abel S, Dubey BN, Schirmer T, Hiller S, Jenal U. 2015. Cyclic di-GMP acts as a cell cycle oscillator to drive chromosome replication. Nature 523:236–239. https://doi.org/10.1038/nature14473.

56. Sprecher KS, Hug I, Nesper J, Potthoff E, Mahi M-A, Sangermani M, Kaever V, Schwede T, Vorholt J, Jenal U. 2017. Cohesive properties of the Caulobacter crescentus holdfast adhesin are regulated by a novel c-di-GMP effector protein. mBio 8:e00294-17. https://doi.org/10.1128/mBio .00294-17.

57. Aldridge P, Paul R, Goymer P, Rainey P, Jenal U. 2003. Role of the GGDEF regulator PleD in polar development of Caulobacter crescentus. Mol Microbiol 47:1695–1708. https://doi.org/10.1046/j.1365-2958.2003.03401.x.

58. Hecht GB, Newton A. 1995. Identification of a novel response regulator required for the swarmer-to-stalked-cell transition in Caulobacter crescentus. J Bacteriol 177:6223–6229. https://doi.org/10.1128/jb.177.21.6223 -6229.1995.

59. Zhou J, Sharp LL, Tang HL, Lloyd SA, Billings S, Braun TF, Blair DF. 1998. Function of protonatable residues in the flagellar motor of Escherichia coli: a critical role for Asp32 of MotB. J Bacteriol 180:2729–2735. https:// doi.org/10.1128/JB.180.10.2729-2735.1998.

60. Alberti L, Harshey RM. 1990. Differentiation of Serratia marcescens 274 into swimmer and swarmer cells. J Bacteriol 172:4322–4328. https://doi .org/10.1128/jb.172.8.4322-4328.1990.

61. Kawagishi I, Imagawa M, Imae Y, McCarter L, Homma M. 1996. The sodium-driven polar flagellar motor of marine Vibrio as the mechanosensor that regulates lateral flagellar expression. Mol Microbiol 20:693–699. https://doi.org/10.1111/j.1365-2958.1996.tb02509.x.

62. Laventie B-J, Sangermani M, Estermann F, Manfredi P, Planes R, Hug I, Jaeger T, Meunier E, Broz P, Jenal U. 2019. A surface-induced asymmetric program promotes tissue colonization by Pseudomonas aeruginosa. Cell Host Microbe 25:140–152.e6. https://doi.org/10.1016/j.chom.2018.11.008.

63. Laganenka L, López ME, Colin R, Sourjik V. 2020. Flagellum-mediated mechanosensing and RflP control motility state of pathogenic Escherichia coli. mBio 11:e02269-19. https://doi.org/10.1128/mBio.02269-19.

64. Güvener ZT, Harwood CS. 2007. Subcellular location characteristics of the Pseudomonas aeruginosa GGDEF protein, WspR, indicate that it produces cyclic-di-GMP in response to growth on surfaces. Mol Microbiol 66:1459–1473. https://doi.org/10.1111/j.1365-2958.2007.06008.x.

65. Luo Y, Zhao K, Baker AE, Kuchma SL, Coggan KA, Wolfgang MC, Wong GCL, O'Toole GA. 2015. A hierarchical cascade of second messengers regulates Pseudomonas aeruginosa surface behaviors. mBio 6:e02456-14. https://doi.org/10.1128/mBio.02456-14.

66. Belas R, Suvanasuthi R. 2005. The ability of Proteus mirabilis to sense surfaces and regulate virulence gene expression involves FliL, a flagellar basal body protein. J Bacteriol 187:6789–6803. https://doi.org/10.1128/JB.187 .19.6789-6803.2005.

67. Tipping MJ, Delalez NJ, Lim R, Berry RM, Armitage JP. 2013. Load-dependent assembly of the bacterial flagellar motor. mBio 4:e00551-13. https:// doi.org/10.1128/mBio.00551-13.

68. Partridge JD, Nieto V, Harshey RM. 2015. A new player at the flagellar motor: FliL Controls both motor output and bias. mBio 6:e02367-14. https://doi.org/10.1128/mBio.02367-14.

69. Hughes KT, Berg HC. 2017. The bacterium has landed. Science 358:446–447. https://doi.org/10.1126/science.aaq0143.

70. Wu DC, Zamorano-Sánchez D, Pagliai FA, Park JH, Floyd KA, Lee CK, Kitts G, Rose CB, Bilotta EM, Wong GCL, Yildiz FH. 2020. Reciprocal c-di-GMP signaling: incomplete flagellum biogenesis triggers c-di-GMP signaling pathways that promote biofilm formation. PLoS Genet 16:e1008703. https://doi.org/10.1371/journal.pgen.1008703.

71. Harrison JJ, Almblad H, Irie Y, Wolter DJ, Eggleston HC, Randall TE, Kitzman JO, Stackhouse B, Emerson JC, Mcnamara S, Larsen TJ, Shendure J, Hoffman LR, Wozniak DJ, Parsek MR. 2020. Elevated exopolysaccharide levels in Pseudomonas aeruginosa flagellar mutants have implications for biofilm growth and chronic infections. PLoS Genet 16:e1008848. https:// doi.org/10.1371/journal.pgen.1008848.

72. Radhakrishnan SK, Thanbichler M, Viollier PH. 2008. The dynamic interplay between a cell fate determinant and a lysozyme homolog drives the asymmetric division cycle of Caulobacter crescentus. Genes Dev 22:212–225. https://doi.org/10.1101/gad.1601808.

73. Janakiraman B, Mignolet J, Narayanan S, Viollier PH, Radhakrishnan SK. 2016. In-phase oscillation of global regulons is orchestrated by a pole-specific organizer. Proc Natl Acad Sci U S A 113:12550–12555. https://doi .org/10.1073/pnas.1610723113.

74. Mignolet J, Holden S, Bergé M, Panis G, Eroglu E, Théraulaz L, Manley S, Viollier PH. 2016. Functional dichotomy and distinct nanoscale assemblies of a cell cycle-controlled bipolar zinc-finger regulator. Elife 5:e20640-21. https://doi.org/10.7554/eLife.18647.

75. Tan MH, Kozdon JB, Shen X, Shapiro L, McAdams HH. 2010. An essential transcription factor, SciP, enhances robustness of Caulobacter cell cycle

regulation. Proc Natl Acad Sci U S A 107:18985–18990. https://doi.org/10.1073/pnas.1014395107.

76. Anderson DK, Ohta N, Wu J, Newton A. 1995. Regulation of the *Caulobacter crescentus rpoN* gene and function of the purified σ54 in flagellar gene transcription. Mol Gen Genet 246:697–706. https://doi.org/10.1007/BF00290715.

77. Aldridge P, Jenal U. 1999. Cell cycle-dependent degradation of a flagellar motor component requires a novel-type response regulator. Mol Microbiol 32:379–391. https://doi.org/10.1046/j.1365-2958.1999.01358.x.

78. Baker AE, Webster SS, Diepold A, Kuchma SL, Bordeleau E, Armitage JP, O'Toole GA. 2019. Flagellar stators stimulate c-di-GMP production by *Pseudomonas aeruginosa*. J Bacteriol 201:263. https://doi.org/10.1128/JB.00741-18.

79. Toutain CM, Zegans ME, O'Toole GA. 2005. Evidence for two flagellar stators and their role in the motility of *Pseudomonas aeruginosa*. J Bacteriol 187:771–777. https://doi.org/10.1128/JB.187.2.771-777.2005.

80. Quon KC, Marczynski GT, Shapiro L. 1996. Cell cycle control by an essential bacterial two-component signal transduction protein. Cell 84:83–93. https://doi.org/10.1016/s0092-8674(00)80995-2.

81. Kaczmarczyk A, Hempel AM, von Arx C, Böhm R, Dubey BN, Nesper J, Schirmer T, Hiller S, Jenal U. 2020. Precise timing of transcription by c-di-GMP coordinates cell cycle and morphogenesis in *Caulobacter*. Nat Commun 11:816. https://doi.org/10.1038/s41467-020-14585-6.

82. Gibson DG, Young L, Chuang R-Y, Venter JC, Hutchison CA, Smith HO.

2009. Enzymatic assembly of DNA molecules up to several hundred kilobases. Nat Methods 6:343–345. https://doi.org/10.1038/nmeth.1318.

83. Ely B. 1991. Genetics of *Caulobacter crescentus*. Methods Enzymol 204:372–384. https://doi.org/10.1016/0076-6879(91)04019-K.

84. Thanbichler M, Iniesta AA, Shapiro L. 2007. A comprehensive set of plasmids for vanillate- and xylose-inducible gene expression in *Caulobacter crescentus*. Nucleic Acids Res 35:e137. https://doi.org/10.1093/nar/gkm818.

85. Wetmore KM, Price MN, Waters RJ, Lamson JS, He J, Hoover CA, Blow MJ, Bristow J, Butland G, Arkin AP, Deutschbauer A. 2015. Rapid quantification of mutant fitness in diverse bacteria by sequencing randomly bar-coded transposons. mBio 6:e00306-15. https://doi.org/10.1128/mBio.00306-15.

86. Kent WJ. 2002. BLAT: the BLAST-like alignment tool. Genome Res 12:656–664. https://doi.org/10.1101/gr.229202.

87. Barrick JE, Colburn G, Deatherage DE, Traverse CC, Strand MD, Borges JJ, Knoester DB, Reba A, Meyer AG. 2014. Identifying structural variation in haploid microbial genomes from short-read resequencing data using breseq. BMC Genomics 15:1039. https://doi.org/10.1186/1471-2164-15-1039.

88. Soding J, Biegert A, Lupas AN. 2005. The HHpred interactive server for protein homology detection and structure prediction. Nucleic Acids Res 33:W244–W248. https://doi.org/10.1093/nar/gki408.

89. Kelley LA, Mezulis S, Yates CM, Wass MN, Sternberg MJE. 2015. The Phyre2 web portal for protein modeling, prediction, and analysis. Nat Protoc 10:845–858. https://doi.org/10.1038/nprot.2015.053.